ECOLOGY

Disentangling the effects of vapor pressure deficit on northern terrestrial vegetation productivity

Ziqian Zhong[1], Bin He[1]*, Ying-Ping Wang[2], Hans W. Chen[3], Deliang Chen[4], Yongshuo H. Fu[5], Yaning Chen[6], Lanlan Guo[7], Ying Deng[8], Ling Huang[9], Wenping Yuan[10], Xingmin Hao[6], Rui Tang[1], Huiming Liu[11], Liying Sun[12], Xiaoming Xie[1], Yafeng Zhang[1]

The impact of atmospheric vapor pressure deficit (VPD) on plant photosynthesis has long been acknowledged, but large interactions with air temperature (T) and soil moisture (SM) still hinder a complete understanding of the influence of VPD on vegetation production across various climate zones. Here, we found a diverging response of productivity to VPD in the Northern Hemisphere by excluding interactive effects of VPD with T and SM. The interactions between VPD and T/SM not only offset the potential positive impact of warming on vegetation productivity but also amplifies the negative effect of soil drying. Notably, for high-latitude ecosystems, there occurs a pronounced shift in vegetation productivity's response to VPD during the growing season when VPD surpasses a threshold of 3.5 to 4.0 hectopascals. These results yield previously unknown insights into the role of VPD in terrestrial ecosystems and enhance our comprehension of the terrestrial carbon cycle's response to global warming.

INTRODUCTION

Atmospheric vapor pressure deficit (VPD), defined as the difference between the saturated vapor pressure and actual vapor pressure, is an important factor influencing stomatal conductance and therefore photosynthesis (*1*, *2*). Plants close their stomata to prevent excessive water loss when VPD is high, and thus, the photosynthesis and carbon uptake of plants are reduced (*1*–*4*). Several studies showed that an increase in VPD substantially influenced vegetation productivity (*1*–*4*), forest mortality (*3*, *5*), crop yields (*6*, *7*), and global terrestrial carbon sinks (*8*). Considering the likely increase in VPD under global warming, VPD will play an increasing role in controlling global ecosystem, carbon, and water exchanges (*2*, *9*).

Changes in VPD can be caused by moisture content in the air and air temperature (T). Evapotranspiration is controlled by soil moisture (SM) among other factors, providing an important source of atmospheric moisture. Therefore, the impact of VPD on vegetation productivity can be driven directly and indirectly through SM and air T. Despite the wide attention given to the effects of VPD on ecosystems, a question that remains open is to what extent vegetation productivity at the regional scale and in different climate zones is influenced by VPD. The difficulty in answering this question lies in the fact that VPD is closely coupled to T and SM, which also have strong influences on terrestrial vegetation productivity. According to the Clausius-Clapeyron relation, the saturated vapor pressure is determined entirely by T (*10*, *11*); therefore, the high correlation between VPD and T is expected. In contrast to the generally negative impact of VPD on vegetation productivity, the impact of T on vegetation productivity is more complex (*12*, *13*). SM is another factor strongly coupled with VPD due to land-atmosphere interactions (*14*, *15*), and can constrain plant photosynthesis directly because it determines the amount of water that can be extracted by plant roots (*16*). Simultaneously, increased VPD associated with decreased SM also affects photosynthesis by regulating the plant stomatal opening (*17*–*19*). To date, the relative effects of VPD, T, and SM on vegetation production remain debated and are difficult to disentangle, while identification of these effects is important to gain a better understanding of the response of vegetation productivity to climate change and improving terrestrial ecosystem models.

In this study, we analyzed the independent effects of VPD on vegetation productivity over the Northern Hemisphere (NH) after excluding the effects caused by T and SM. Satellite observation-based contiguous solar-induced fluorescence (CSIF) and leaf area index (LAI), as well as gross primary productivity simulated from empirical models based on eddy covariance observational data (GPP-FLUXCOM), were used as proxies for vegetation productivity. To quantify the independent influences of VPD, we first used ridge regression analysis to eliminate the interactions between VPD and T or SM and assessed the response of vegetation productivity to VPD at the interannual scale using growing-season mean values. Here, T and VPD were sourced from the fifth generation ECMWF reanalysis (ERA5) dataset (*20*), and SM was obtained from the Global Land Evaporation Amsterdam Model (GLEAM) dataset (*21*). The vegetation growing season was defined as those months with an average T higher than 0°C (*22*). We then applied

[1]State Key Laboratory of Earth Surface Processes and Resource Ecology, Faculty of Geographical Science, Beijing Normal University, 100875 Beijing, China. [2]CSIRO Environment, Private Bag 1, Aspendale, Victoria, Australia. [3]Department of Space, Earth and Environment, Division of Geoscience and Remote Sensing, Chalmers University of Technology, SE-412 96 Gothenburg, Sweden. [4]Regional Climate Group, Department of Earth Sciences, University of Gothenburg, S-40530 Gothenburg, Sweden. [5]College of Water Sciences, Beijing Normal University, 100875 Beijing, China. [6]State Key Laboratory of Desert and Oasis Ecology, Xinjiang Institute of Ecology and Geography, Chinese Academy of Sciences, 830011 Urumqi, China. [7]School of Geography, Beijing Normal University, 100875 Beijing, China. [8]State Key Laboratory of Vegetation and Environmental Change, Institute of Botany, Chinese Academy of Sciences, No. 20 Nanxincun, Xiangshan, 100093 Beijing, China. [9]College of Urban and Environmental Sciences, Peking University, 100871 Beijing, China. [10]School of Atmospheric Sciences, Sun Yat-Sen University, 510275 Guangzhou, China. [11]Ministry of Ecology and Environment Center for Satellite Application on Ecology and Environment, 100094 Beijing, China. [12]Key Laboratory of Water Cycle and Related Land Surface Processes, Institute of Geographic Sciences and Natural Resources Research, Chinese Academy of Sciences, 100101 Beijing, China.
*Corresponding author. Email: hebin@bnu.edu.cn

a structural equation model with the partial least square (PLS-SEM) algorithm to disentangle the direct effect of VPD on vegetation from the indirect effects of T or SM on vegetation via VPD.

RESULTS

The independent effects of VPD on vegetation productivity

The independent effect refers to the impact of an independent variable on the dependent variable after excluding confounding effects of other independent variables (*23*, *24*). In this study, the independent effect of VPD on GPP represents the magnitude of GPP change resulting from variations in VPD while controlling for the effects of other environmental factors that may also influence GPP, such as T and SM. High degrees of multicollinearity among VPD, SM, and T have posed challenges to quantifying the independent effect of VPD on GPP. High multicollinearity is evident in the notable correlations between the average growing-season VPD and SM or T (fig. S1A and B). In addition, high variance inflation factors (VIFs; see Materials and Methods) are found in most areas across the NH for a multiple linear regression with an average growing-season SM, T, VPD, and solar radiation (R) as independent variables and an average growing-season CSIF as the dependent variable (fig. S1C), reinforcing this issue. In this analysis, the effect of solar radiation on vegetation productivity was considered as there is a direct correlation between solar radiation and plant photosynthesis. These high degrees of multicollinearity among independent variables have the potential to result in substantial regression coefficient bias and misleading statistical inferences (*23*, *25*).

To reduce the impact of multicollinearity on the correct detection of the relationships, we performed a ridge regression analysis (*26*) to assess the effect of the average growing-season VPD on CSIF. Ridge regression is a linear regularization method and an effective eliminator of multicollinearity. It improves upon the ordinary least square regression model in scenarios where the independent variables are strongly correlated by introducing a penalty term in the cost function, which penalizes large parameter values. Thus, it is appropriate for analysis when there exists severe multicollinearity among independent variables. As shown in fig. S1D, the VIFs of the ridge regression model are much smaller than that of the original multivariate linear model, indicating that the interactions among SM, T, and VPD were minimized and that the regression coefficients of the ridge regression model offered more reliable information about the influences of the independent variables than that of the multiple linear regression model.

On the basis of the ridge regression analysis using average annual growing-season values, a distinct contrast in the independent effect of VPD on CSIF is observed between arid and humid zones (Fig. 1). In most middle- and low-latitude regions, such as Central Asia, western North America, and India, the CSIF was negatively correlated with VPD, which is consistent with the negative responses of surface conductance or photosynthesis to increases in VPD (*2*, *27*). In contrast, CSIF was positively correlated with VPD in some boreal zones, such as northern Eurasia and northern North America. Similar results were also found over the NH when using GPP-FLUXCOM (1980–2018) and LAI–Moderate Resolution Imaging Spectroradiometer (MODIS) (2001–2019) as proxies for vegetation productivity instead of CSIF (fig. S2) or when substituting SM data obtained from the ERA5 dataset instead of the GLEAM dataset (fig. S3). To test the robustness of our analysis, we also applied an additional statistical analysis called principal component regression (*28*). Principal component regression produces principal components (PCs) that are orthogonal (i.e., uncorrelated) to each other in the regression, enabling optimal performance with highly correlated predictor variables. This method reveals a consistent pattern in the response of vegetation productivity proxies (CSIF, GPP-FLUXCOM, and LAI-MODIS) to VPD, with a notable variation found in the independent impact of VPD on productivity among different climate zones (fig. S4). Both regression methods demonstrate that vegetation productivity shows a negative response to VPD changes in arid and semiarid zones while exhibiting neutral or positive responses in humid zones.

The role of VPD in vegetation production

The above analysis suggests that VPD changes alone extensively affected vegetation productivity during 2000–2019. In the real world, however, VPD is considered the middle variable of T or SM variations affecting vegetation productivity. For example, rising T could lead to higher VPD and thereby further limit plant photosynthesis. In addition, when soil becomes wetter, the increasing evaporation reduces VPD and further promotes plant transpiration and photosynthesis. These different processes imply simultaneously multiple pathways for VPD to influence vegetation productivity by interacting with other variables, such as T and SM. To further reveal how T and SM have influenced vegetation production via VPD, a PLS-SEM model (see Materials and Methods) was used to detect the direct and indirect effects of average growing-season climatic variables and SM on vegetation productivity. Figure 2A shows all pathways of how the environmental variables (SM, T, VPD, and solar radiation) can affect CSIF in the PLS-SEM model. Here, we used goodness of fit (GoF), an index for assessing the overall prediction performance of the model, to measure the model reliability (Fig. 2B). Only grid cells with a GoF larger than 0.5 from the PLS-SEM results were considered in the analyses following a previous study (*29*). The effect of environmental factors on vegetation productivity was quantified using the derived influence coefficients from the PLS-SEM model, where a high positive influence coefficient indicates a strong positive effect. The strengths of the direct effects were given by the path coefficients, which represent the direction and strength of the linear relationships between variables. An indirect effect is the influence of one predictor on another response variable by taking an indirect path, namely, adding the product of all possible paths excluding the direct effect (*29*). The total effect is defined as the sum of direct effects and indirect effects.

To detect what role VPD has played in affecting vegetation productivity, we compared and quantified the direct effect of T on CSIF with the indirect effect of T on CSIF via VPD during 2000–2019. The interactions between the direct effect of average growing-season T (Di.) and indirect effect of average growing-season T via VPD (In.) on CSIF were divided into four categories: positive Di. and In. (Di+ and In+), positive Di. and negative In. (Di+ and In−), negative Di. and positive In. (Di− and In+), and negative Di. and In. (Di− and In−). When the directions of direct and indirect effects are the same, we call this an enhancing effect and otherwise an offset effect. The degree of enhancing or offset effects could be determined by the absolute value of the ratio (%) of the In. to the Di. influence coefficient in the PLS-SEM model. Here, T exerted a negative, indirect effect on CSIF via VPD across most middle- and low-latitude regions, especially in arid and semiarid

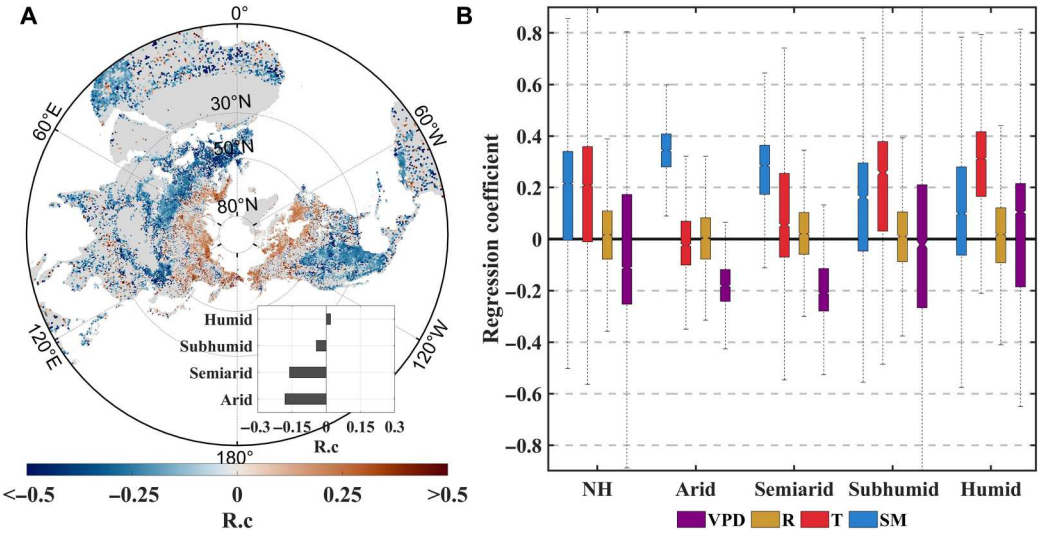

Fig. 1. The independent effect of VPD on vegetation productivity over the NH. (**A**) Ridge regression coefficient (R.c) of VPD to CSIF during the growing season from 2000 to 2019. The inset shows the mean value of the R.c over arid, semiarid, subhumid, and humid zones. (**B**) R.cs for VPD, solar radiation (R), air T, and SM in the regression with CSIF over the different climate zones, visualized with a boxplot. The height of each box indicates the interquartile range, the notch of each box indicates the median, and the bottom and top of the box indicate the first and third quartiles, respectively. The whiskers that extend to the most extreme regression coefficient are not considered outliers, which is a value that is more than 1.5 times the interquartile range away from the bottom or top of the box. Only the grid cells with the regression result that passed the test of significance ($P < 0.05$) were analyzed and are shown.

zones, while a positive indirect effect on CSIF via VPD was observed in the high-latitude region (Fig. 2D). One major interaction was that the negative effect of T on CSIF via VPD offset the positive effect of T on CSIF (Di+ and In−), which accounted for 55.6% of the vegetation area and was mainly distributed in eastern Africa, Europe, Central Asia, India, East Asia, and North America (Fig. 2E). In these areas, vegetation productivity increased with increasing T, while vegetation productivity may also have been supressed by the higher VPD caused by a rising T. We focused on this most widespread interaction and found that the negative effect of T on CSIF via VPD offset had a median magnitude of 69.4% of the positive effect of T on CSIF over the NH (Fig. 2F). This offset effect was strongest in the arid zone (126.7%), followed by that in the semiarid (112.2%), subhumid (62.5%), and humid (39.0%) zones. Here, median values were used to minimize the impact of outliers. Similar results were also found when using LAI-MODIS data that covers a comparable time period (2001–2019) as a proxy for GPP (fig. S5) or when substituting SM data obtained from the ERA5 dataset instead of the GLEAM dataset (fig. S6).

In parallel to the direct and indirect effects of T on CSIF, the direct effect of SM on CSIF and the indirect effect of SM on CSIF via VPD during 2000–2019 were also recognized, as shown in Fig. 3. SM exerted a positive indirect effect on CSIF via VPD across most regions. In contrast to the counteraction between the direct and indirect effects of T on CSIF, the direct positive effect of SM and indirect positive effect of SM via VPD on CSIF (Di+ and In+) reinforced each other in arid and semiarid zones, which respectively accounted for 63.6 and 60.8% of the total vegetated area in these zones, respectively. The process by which SM positively affected CSIF via VPD can be explained by the fact that increased SM could have reduced VPD through increased evaporation and further restrained the negative effects on vegetation brought by high-VPD conditions. The interactions between Di. and In. in humid and semihumid zones were complex (Fig. 3C). Vegetation in these zones was not limited by water availability; therefore, the positive Di. or In. was not prevalent in these areas. Similar results were also found when using LAI-MODIS data as a proxy for GPP during the period 2001 to 2019, as well as when substituting SM data obtained from the ERA5 dataset instead of the GLEAM dataset, as demonstrated by figs. S7 and S8, respectively. The above findings reveal the strong counteraction between the direct effect of T and T-associated VPD effect on CSIF and the enhancement of the direct effect of SM and SM-associated VPD effect on CSIF.

The threshold of VPD sensitivities of vegetation productivity

The results above show diverging sensitivities of productivity to VPD across different climate zones. The shift from a positive to a negative influence of VPD on productivity indicates that there is a VPD threshold that determines the direction of the effect of VPD on vegetation productivity. We hypothesize that VPD positively influenced photosynthesis during the growing season up to a certain VPD threshold, beyond which a shift in the response direction of vegetation productivity to VPD occurred with the increase of VPD. To test this hypothesis, we focused on the interannual effect of VPD on the GPP in high-latitude Eurasia (0° to 180°E, 50° to 85°N), where we detected the positive effect of VPD on vegetation productivity based on the ridge regression analysis (Fig. 1A) and PLS-SEM analysis (Fig. 2D). As depicted in the insets of Fig. 4, we investigated the ridge regression coefficient (R.c) between VPD and interannual variations of GPP-FLUXCOM or CSIF during the growing season. The median of R.c changed modestly at first and declined significantly above a certain VPD threshold. The average growing-season VPD threshold, which was defined as breakpoints (BPs) of the medians in Fig. 4, was identified by the

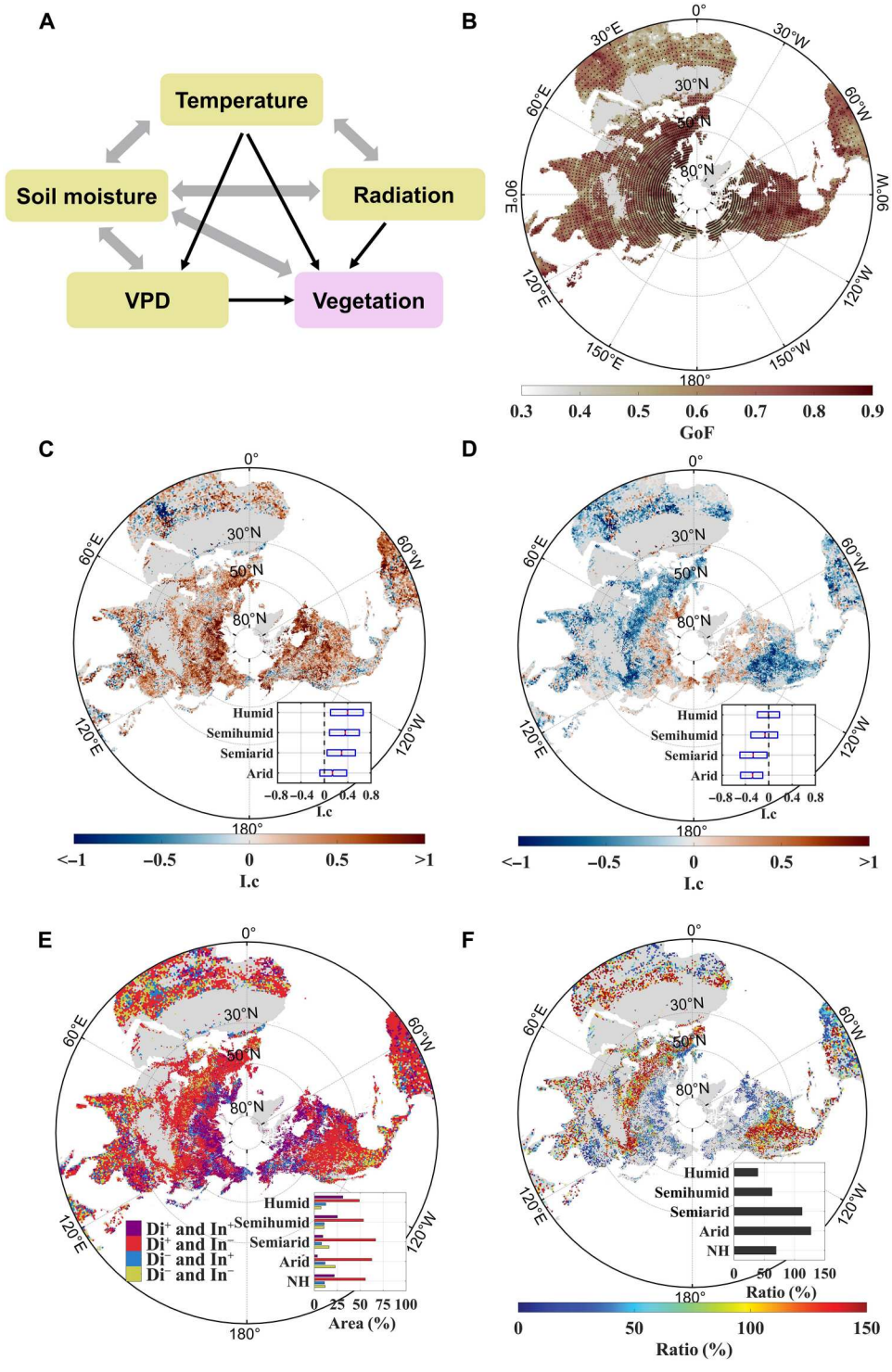

Fig. 2. The offset effect of the influence of VPD on vegetation productivity compared to the air T effect on vegetation productivity. (**A**) Conceptual model depicting hypothesized direct and indirect effects of T, SM, R, and VPD on vegetation productivity, which was represented by CSIF. Double-headed gray arrows indicate covariance between the variables, and single-headed black arrows indicate the hypothesized direction of causation. (**B**) GoF of PLS-SEM with CSIF as the vegetation productivity proxies during the growing season from 2000 to 2019. The dots indicate the pixels with a GoF of PLS-SEM larger than 0.5. (**C**) Direct effect of T on CSIF (Di.) and (**D**) the indirect effect of T on CSIF via VPD (In.) during the growing season from 2000 to 2019. The effects were quantified using the derived influence coefficients (I.cs) from the PLS-SEM model, which were visualized with a boxplot. The width of each box indicates the interquartile range of I.c for all grid points, the red line in each box indicates the median, and the left and right edges of the box indicate the first and third quartiles, respectively. (**E**) Interaction between positive or negative Di. (Di+ or Di−) and positive or negative In. (In+ or In−) on CSIF. The insets show the area proportion (%) of different categories of interaction over the whole NH and different climate zones. (**F**) Degree of offset effect (ratio) between Di+ and In−. Only the regions in (E) with Di+ and In− were selected and analyzed. The insets show the median of the ratio in the grid points over different climate zones.

nonparametric Pettitt breakpoint test (*30*) as 3.50 hPa ($P < 0.01$) and 3.96 hPa ($P < 0.01$) derived from the GPP-FLUXCOM and CSIF data, respectively. Above the VPD threshold, the positive sensitivity of vegetation productivity declined substantially. Similar results were also found when ridge regression analysis was performed using the SM data obtained from the ERA5 dataset instead of the GLEAM dataset (fig. S9) or when the independent effect of VPD on vegetation productivity proxy was estimated by principal component regression (fig. S10).

DISCUSSION

In this study, we found that there were differences in the sensitivity of productivity to VPD across different climate zones, although it is

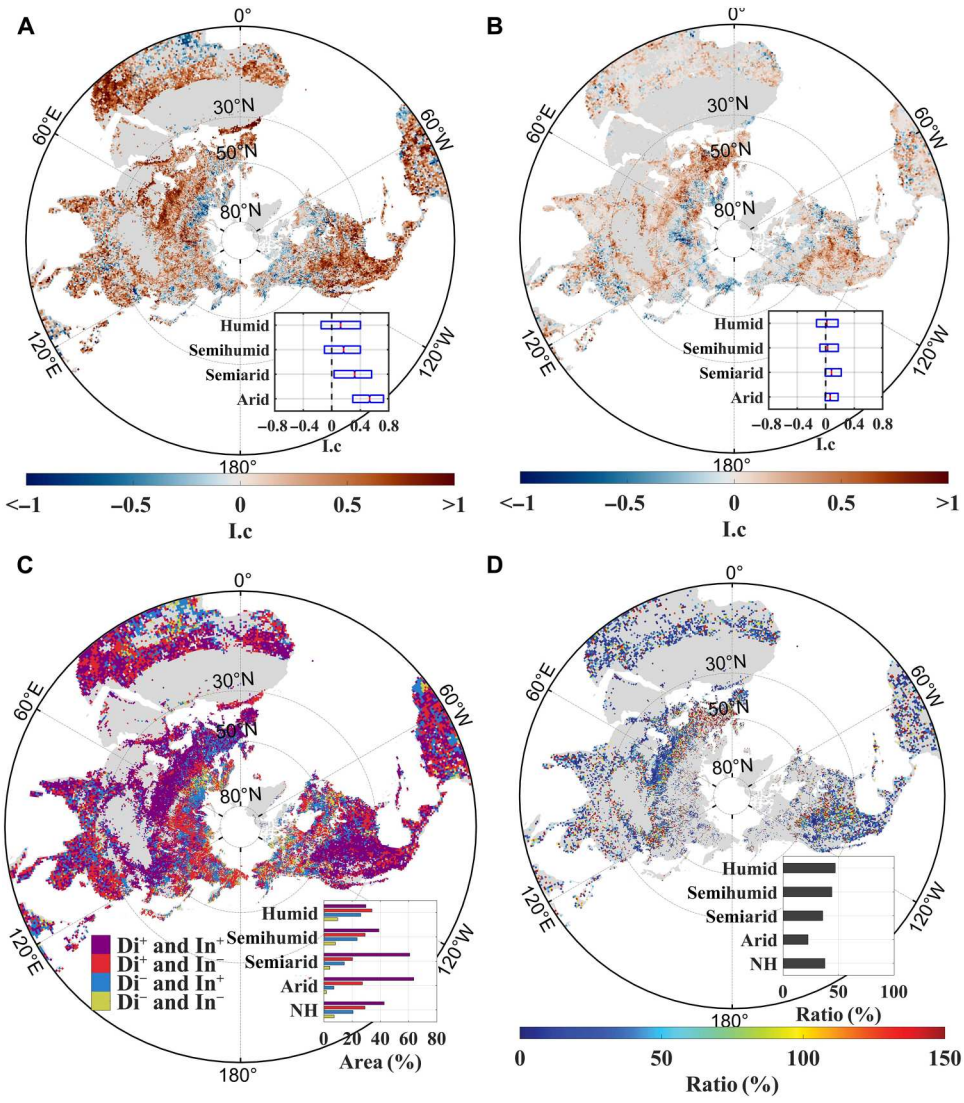

Fig. 3. The enhancing effect of the influence of VPD on vegetation productivity to the influence of SM on vegetation productivity. (**A**) Direct effect of SM on CSIF (Di.) and (**B**) the indirect effect of SM on CSIF via VPD (In.) during the growing season from 2000 to 2019. The effects were quantified using the derived I.cs from the PLS-SEM model, which were visualized with a boxplot. The width of each box indicates the interquartile range of I.c for grid points, the red line in each box indicates the median, and the left and right edges of the box indicate the first and third quartiles, respectively. (**C**) Interaction between positive or negative Di. (Di+ or Di−) and positive or negative In. (In+ or In−) on CSIF. The inset shows the area proportion (%) of different categories of interaction over the whole NH and different climate zones. (**D**) Degree of enhancing effect (ratio) between Di+ and In+. Only the regions in (C) with Di+ and In+ were selected and analyzed. The inset shows the median of the ratio in the grid points over different climate zones.

well known that increasing VPD alone reduces stomatal conductance and further inhibits photosynthesis under conditions of high VPD. By contrast, however, some leaf-scale studies have suggested that the stomatal conductance of leaves increases with increasing VPD (*31*, *32*) and thus leads to an increased photosynthetic rate under conditions of low VPD (*33*, *34*). When VPD is low and the stomata are fully open, the leaf guard cells sense the increased rate of transpiration through the stomatal pores and induce stomatal opening (*35*). As a result of this "feedback" response (*36*), with an increase of VPD, the transpiration rate increases and the nutrient (such as nitrogen, phosphorus, and potassium) uptake from the soil is promoted (*37*–*40*), which is beneficial for vegetation growth. Moreover, some field experiments performed in northern Europe where the positive effect of VPD on vegetation productivity was detected (Fig. 1A) revealed adverse effects of an increase in atmospheric humidity (or decrease in VPD) on photosynthetic capacity and growth rate in vegetation. The adverse impact includes reducing branch and stem wood density and diminishing nutrient supply to foliage (*34*), reducing glandular trichome density (*39*), and reducing intrinsic water-use efficiency, which could expose plants to a greater risk of dehydration under water stress (*41*). These factors could explain the neutral or even positive effects of VPD on vegetation in regions with generally low VPD, such as northern Eurasia.

The varying responses of vegetation productivity to VPD in dry and moist regions result in a rapid shift toward negative responses

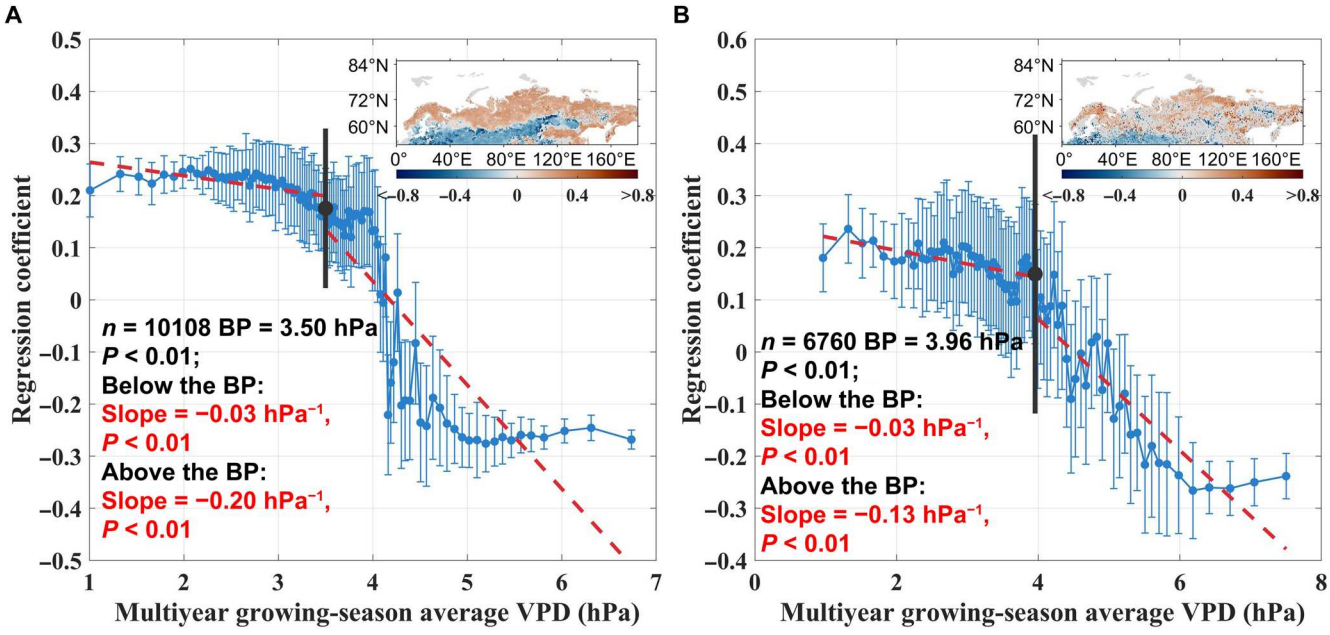

Fig. 4. The thresholds in the relationship between VPD and the sensitivity of vegetation productivity to VPD for high-latitude ecosystems. The R.c of average growing-season VPD to average growing-season vegetation productivity proxies, which were (**A**) GPP-FLUXCOM (during 1980–2018) and (**B**) CSIF (during 2000–2019) as a function of multiyear growing-season average VPD in high-latitude Eurasia (0° to 180°E, 50° to 85°N). The blue points and error bars represent the median and SD of R.c in each bin, respectively (see Materials and Methods). The nonparametric Pettitt test was used to detect the occurrence of BPs in the medians, which are shown as black points and heavy lines. The red dotted line represents the line-fitting curve of medians below or above the BP. The insets show the spatial pattern of the regression coefficient of VPD to vegetation productivity proxies during the growing season. Only the grid cells with the regression result that passed the test of significance ($P < 0.05$) were analyzed and shown.

once the atmospheric aridity level surpasses a critical threshold at the vegetation location. This study identifies a VPD threshold specific to high-latitude ecosystems, which is strongly correlated with the local climatic conditions in the vegetation region. In addition, this finding suggests that there may be differences in vegetation stomatal responses to VPD in various levels of atmospheric dryness. To investigate the potential mechanism behind this VPD threshold, we conducted ridge regression analysis using average growing-season VPD, SM, T, solar radiation, wind speed, and GPP-FLUXCOM as independent variables as well as average growing-season transpiration rate as the dependent variable in the northern Eurasia region (fig. S11). Here, we examined the relationship between VPD and transpiration rate because the rate of transpiration is directly related to stomatal conductance (*42*–*45*). When the average VPD during the growing season was below the threshold of 3.85 hPa, the transpiration rate showed a positive sensitivity to VPD, and the sensitivity value slightly increased with the increase of environmental VPD. This suggests that plant stomata were fully open, in accordance with previous studies that also observed stomatal opening under low VPD conditions (*46*, *47*). Consequently, it is possible that photosynthesis was not barely restricted by VPD. Above the VPD threshold, the positive sensitivity of transpiration rate declined considerably. This indicates that leaf stomatal conductance was starting to be substantially limited by VPD, leading to a corresponding inhibition of photosynthesis. The threshold effect of stomatal conductance in response to VPD has been documented in previous experimental studies (*31*, *48*, *49*). Nonetheless, it should be noted that the threshold may vary considerably among different plant species. This variation could be attributed to differences in stomatal regulation capacity, which varies among species (*50*–*53*).

We further investigated how water stress affected the sensitivity of GPP to VPD by exploring the relationship between GPP and VPD under different average growing-season VPD and SM conditions (fig. S12). Above a greater VPD threshold, negative GPP response to VPD was observed under conditions of higher SM. Under conditions of increasing VPD, sufficient SM enables vegetation to maintain high transpiration efficiency, which can reduce the impact of VPD on leaf stomatal conductance and vegetation photosynthesis. These findings support the notion that plants balance various costs, such as productivity and leaf T regulation during drought, by operating stomata at the edge of the supply capacity of the plant's hydraulic system (*54*–*56*). However, we found that the pattern of GPP sensitivity to VPD varied more substantially with changes in the average growing-season VPD overall compared to the influence of SM. Negative GPP response to VPD is common when the average VPD during the growing season is 4 hPa or higher, regardless of SM conditions. This pattern highlights the critical role of VPD background values in determining the response of GPP to VPD.

Our hemispheric-scale analysis of the influence of VPD as an independent variable on vegetation productivity was an attempt to identify what role VPD in isolation plays in influencing vegetation production and to what extent it affects vegetation production. We found that VPD in isolation had a strong impact on vegetation productivity and revealed the strong counteraction between the direct effect of T and T-associated VPD effect on vegetation productivity and the enhancing effect of the direct effect of SM and SM-

associated VPD effect on the vegetation productivity in most parts of the NH. In addition, we proposed and accepted a hypothesis that there exists an average growing-season VPD threshold of the sensitivity of vegetation productivity to VPD, which led to the positive response of vegetation productivity to VPD in low VPD regions, such as high-latitude ecosystems, and the negative response of vegetation productivity to VPD in other parts of the NH with higher VPD. Our findings provide insights into the role VPD plays in terrestrial ecosystems, disentangle the interaction between VPD and T or SM on vegetation productivity, and reveal the potential threat of prospective increasing VPD under global warming (*2*, *57*) in high-latitude ecosystems.

Note that, however, the extent to which VPD affects ecosystems is still highly uncertain due to the possible carryover effect (*58*) of climatic factors on terrestrial ecosystems. More in-depth studies using datasets with different time scales are needed in the future to more accurately assess the impact of VPD on vegetation productivity. In addition, station-based analysis is needed to further detect more exact values of the VPD threshold for different ecosystems and to further reveal the mechanism for the positive response of vegetation productivity to VPD under wetter conditions (*59*). Continuous monitoring and dedicated experiments could improve our understanding of the role of VPD in terrestrial ecosystems.

MATERIALS AND METHODS

Vegetation productivity

The CSIF dataset (*60*), LAI-MODIS dataset, and GPP derived from empirical models based on flux tower observations (FLUXCOM) were used to indicate vegetation productivity in this study. The clear-sky condition CSIF dataset was generated at moderate spatio-temporal resolutions (0.05° × 0.05° and 4 days) and over the 2000–2019 period by training a neural network with surface reflectance from the MODIS reflectance dataset (MCD43C4 V006) and SIF from the Orbiting Carbon Observatory-2 (OCO-2). The CSIF not only shows high accuracy when validated against the satellite-retrieved OCO-2 SIF but also exhibits a strong correlation with GPP estimated from flux towers. The MOD15A2H Version 6 MODIS combined with LAI and fraction of photosynthetically active radiation product is an 8-day composite dataset with a 500-m pixel size available from 2000. The algorithm chooses the "best" pixel available from all acquisitions of the Terra sensor within the 8-day period. The FLUXCOM GPP with a spatial resolution of 0.5° × 0.5° is a monthly dataset simulated from empirical models forced by eddy covariance data, remote sensing data, and climate data (*61*). The empirical models were trained by random forests, artificial neural networks, and multivariate adaptive regression spline algorithms. Here, the FLXUCOM carbon fluxes data driven by the ERA5 climate reanalysis from 1980 to 2018 were used. All datasets were aggregated to a spatial resolution of 0.5° before analysis.

Climate, SM, and transpiration data

The monthly root-zone SM and transpiration at a spatial resolution of 0.25° were obtained from the Global Land Evaporation Amsterdam Model (GLEAM) version 3.5 datasets, which is a global dataset spanning the 41-year period from 1980 to 2020 and based on satellite and reanalysis data. The monthly 2-m air T, dew point T, 10-m wind speed, and SM were obtained from the ERA5 for the global climate and weather with a spatial resolution of 31 km. Here, SM content between 0 and 1 m was calculated by summing up the moisture content for each layer and weighting it by the thickness of the layer (*16*). The monthly surface net downward shortwave radiation at a spatial resolution of 0.625° × 0.5° was obtained from the Modern-Era Retrospective analysis for Research and Applications, Version 2 (MERRA-2) datasets beginning in 1980 (*62*). According to the Clausius-Clapeyron relation, we used monthly 2-m T and dew point data to calculate VPD based on the ERA5 dataset (*27*). All datasets were aggregated to a spatial resolution of 0.5°.

Aridity index

The aridity index (AI), defined as the ratio of annual precipitation to annual potential evapotranspiration, was used to identify global climate zones. Under this quantitative indicator, the NH was classified into arid (AI < 0.2), semiarid (0.2 ≤ AI < 0.5), subhumid (0.5 ≤ AI < 0.65), and humid (AI ≥ 0.65) subtypes. The AI was obtained from the Global Aridity Index and Potential Evapotranspiration (ET0) Climate Database v2 (*63*).

Pearson's correlation analysis

Pearson's correlation analysis between VPD and SM or T was used to determine the coupling between VPD and SM and T. The significance of Pearson's correlations was assessed at $P < 0.05$.

Ridge regression analysis

To account for multicollinearity among VPD, T, and SM, we performed a ridge regression analysis to verify the effect of VPD on vegetation productivity. Ridge regression is a widely used linear regularization method and independent statistical test commonly used in plant physiology and ecophysiology, which improves the mean square error of estimation by introducing a penalty term in the minimized residual equation, and substantially increases the reliability of the estimates in cases of strong multicollinearity. Because the advantage of ridge regression, it is widely used in the research of the response of the ecosystem to changes in climate variables, especially in the regression analysis when there exists severe multicollinearity among climate variables [e.g., severe multicollinearity among daytime warming and night-time warming (*24*) or seasonal mean T and precipitation (*64*)]. The VIF, which assesses how much the variance of an estimated regression coefficient increases when predictors are correlated, is used to detect the severity of multicollinearity in the regression analysis. When notable multicollinearity issues exist, the VIF will be very large for the variables involved.

In the regression analysis, all variables were normalized with *z* score and detrended using a linear model to focus on the interannual relationship between VPD and vegetation productivity. Because we focused on the relationship among environmental factors, SM, and vegetation, to eliminate the interference of misleading relationships in bare land, only the regions with multiyear (during 2000–2019) average CSIF values larger than 0.006 mW m^{-2} nm^{-1} sr^{-1} were selected for the ridge regression analysis following (*60*). The significance of the ridge regression analysis was assessed using an *F* test at a significance level of 0.05.

Principal component regression analysis

We also used the principal component regression analysis (*28*) to verify the effect of VPD on vegetation productivity. The principal component regression transforms the original dataset into a new set of orthogonal (i.e., uncorrelated) variables, which are called

PCs. After transformation, a least square regression on this reduced set of PCs was performed. The principal component regression avoids collinearity of climatic variables because PCs are uncorrelated to each other. The low-variance PCs indicate collinearity among original predictors and thus should be excluded in the regression step. Here, the PCs that explain less than 5% of the overall variance of climatic variables were excluded from the regression (*64*). Only the regions with multiyear average annual CSIF values larger than 0.006 mW m^{-2} nm^{-1} sr^{-1} were selected for the regression analysis. The significance of the principal component regression analysis was assessed using an F test at a significance level of 0.05.

PLS-SEM

PLS-SEM is a multivariate statistical analysis technique for path analysis that requires previous knowledge to establish the relationships among the variables. In contrast to the common structural equation modeling, which is based on maximum likelihood, PLS-SEM requires neither a large sample size nor a specific assumption on the distribution of the data and works well with missing data. When the sample size and data distribution do not conform to the requirements of common SEMs, for example, when long-term observations are not available, PLS-SEM has a more functional advantage. Here, we ran our PLS-SEM model using 1000 bootstraps to validate the estimates of path coefficients and the coefficients of determination. The degree of direct effect, indirect effect, and total effect can be quantified by the direct influence coefficient, indirect influence coefficient, and total influence coefficient, respectively. Models with different input variables were evaluated using the GoF statistic. GoF assesses the overall prediction performance of the model by considering the commonality and R^2 coefficients. All variables were standardized before conducting the path analysis and were detrended using a linear model in the path analysis to focus on the interannual relationship between environmental factors and vegetation productivity. Only the regions with multiyear (during 2000–2019) average CSIF values larger than 0.006 mW m^{-2} nm^{-1} sr^{-1} were selected for the PLS-SEM analysis.

VPD threshold

To detect the threshold in the relationship between VPD and the sensitivity of vegetation productivity to VPD, all grid points were firstly sorted into $\sqrt{n}$ (rounded to the nearest integer) bins, where n is the number of grid points, according to the ascending order of average growing-season VPD. Then, the VPD threshold, which was defined as BPs of the medians of the groups, was quantified by the nonparametric Pettitt breakpoint test (*30*), which has been widely used to detect abrupt changes in observed climatic and hydrological series (*65*, *66*).

Supplementary Materials

This PDF file includes:

Figs. S1 to S12

REFERENCE AND NOTES

1. B. N. Sulman, D. T. Roman, K. Yi, L. Wang, R. P. Phillips, K. A. Novick, High atmospheric demand for water can limit forest carbon uptake and transpiration as severely as dry soil. *Geophys. Res. Lett.* **43**, 9686–9695 (2016).
2. K. A. Novick, D. L. Ficklin, P. C. Stoy, C. A. Williams, G. Bohrer, A. C. Oishi, S. A. Papuga, P. D. Blanken, A. Noormets, B. N. Sulman, R. L. Scott, L. Wang, R. P. Phillips, The increasing importance of atmospheric demand for ecosystem water and carbon fluxes. *Nat. Clim. Change* **6**, 1023–1027 (2016).
3. A. Park Williams, C. D. Allen, A. K. Macalady, D. Griffin, C. A. Woodhouse, D. M. Meko, T. W. Swetnam, S. A. Rauscher, R. Seager, H. D. Grissino-Mayer, J. S. Dean, E. R. Cook, C. Gangodagamage, M. Cai, N. G. McDowell, Temperature as a potent driver of regional forest drought stress and tree mortality. *Nat. Clim. Change* **3**, 292–297 (2013).
4. K. A. Novick, C. F. Miniat, J. M. Vose, Drought limitations to leaf-level gas exchange: Results from a model linking stomatal optimization and cohesion-tension theory. *Plant Cell Environ.* **39**, 583–596 (2016).
5. D. Eamus, N. Boulain, J. Cleverly, D. D. Breshears, Global change-type drought-induced tree mortality: Vapor pressure deficit is more important than temperature per se in causing decline in tree health. *Ecol. Evol.* **3**, 2711–2729 (2013).
6. D. B. Lobell, G. L. Hammer, G. McLean, C. Messina, M. J. Roberts, W. Schlenker, The critical role of extreme heat for maize production in the United States. *Nat. Clim. Change* **3**, 497–501 (2013).
7. D. Zhang, Q. Du, Z. Zhang, X. Jiao, X. Song, J. Li, Vapour pressure deficit control in relation to water transport and water productivity in greenhouse tomato production during summer. *Sci. Rep.* **7**, 43461 (2017).
8. B. He, C. Chen, S. Lin, W. Yuan, H. W. Chen, D. Chen, Y. Zhang, L. Guo, X. Zhao, X. Liu, S. Piao, Z. Zhong, R. Wang, R. Tang, Worldwide impacts of atmospheric vapor pressure deficit on the interannual variability of terrestrial carbon sinks. *Natl. Sci. Rev.* **9**, nwab150 (2021).
9. J. Ding, T. Yang, Y. Zhao, D. Liu, X. Wang, Y. Yao, S. Peng, T. Wang, S. Piao, Increasingly important role of atmospheric aridity on Tibetan Alpine grasslands. *Geophys. Res. Lett.* **45**, 2852–2859 (2018).
10. C. Yi, E. Pendall, P. Ciais, Focus on extreme events and the carbon cycle. *Environ. Res. Lett.* **10**, 070201 (2015).
11. G. G. Katul, R. Oren, S. Manzoni, C. Higgins, M. B. Parlange, Evapotranspiration: A process driving mass transport and energy exchange in the soil-plant-atmosphere-climate system. *Rev. Geophys.* **50**, 10.1029/2011RG000366, (2012).
12. M. Huang, S. Piao, P. Ciais, J. Peñuelas, X. Wang, T. F. Keenan, S. Peng, J. A. Berry, K. Wang, J. Mao, R. Alkama, A. Cescatti, M. Cuntz, H. De Deurwaerder, M. Gao, Y. He, Y. Liu, Y. Luo, R. B. Myneni, S. Niu, X. Shi, W. Yuan, H. Verbeeck, T. Wang, J. Wu, I. A. Janssens, Air temperature optima of vegetation productivity across global biomes. *Nat. Ecol. Evol.* **3**, 772–779 (2019).
13. Ü. Niinemets, Global-scale climatic controls of leaf dry mass per area, density, and thickness in trees and shrubs. *Ecology* **82**, 453–469 (2001).
14. S. I. Seneviratne, T. Corti, E. L. Davin, M. Hirschi, E. B. Jaeger, I. Lehner, B. Orlowsky, A. J. Teuling, Investigating soil moisture–climate interactions in a changing climate: A review. *Earth-Sci. Rev.* **99**, 125–161 (2010).
15. S. Zhou, Y. Zhang, A. Park Williams, P. Gentine, Projected increases in intensity, frequency, and terrestrial carbon costs of compound drought and aridity events. *Sci. Adv.* **5**, eaau5740 (2019).
16. L. Liu, L. Gudmundsson, M. Hauser, D. Qin, S. Li, S. I. Seneviratne, Soil moisture dominates dryness stress on ecosystem production globally. *Nat. Commun.* **11**, 4892 (2020).
17. B. D. Stocker, J. Zscheischler, T. F. Keenan, I. C. Prentice, J. Peñuelas, S. I. Seneviratne, Quantifying soil moisture impacts on light use efficiency across biomes. *New Phytol.* **218**, 1430–1449 (2018).
18. A. P. Williams, C. D. Allen, C. I. Millar, T. W. Swetnam, J. Michaelsen, C. J. Still, S. W. Leavitt, Forest responses to increasing aridity and warmth in the southwestern United States. *Proc. Natl. Acad. Sci. U.S.A.* **107**, 21289–21294 (2010).
19. L. Liu, S. Peng, A. AghaKouchak, Y. Huang, Y. Li, D. Qin, A. Xie, S. Li, Broad consistency between satellite and vegetation model estimates of net primary productivity across global and regional scales. *J. Geophys. Res. Biogeo.* **123**, 3603–3616 (2018).
20. H. Hersbach, B. Bell, P. Berrisford, S. Hirahara, A. Horányi, J. Muñoz-Sabater, J. Nicolas, C. Peubey, R. Radu, D. Schepers, A. Simmons, C. Soci, S. Abdalla, X. Abellan, G. Balsamo, P. Bechtold, G. Biavati, J. Bidlot, M. Bonavita, G. Chiara, P. Dahlgren, D. Dee, M. Diamantakis, R. Dragani, J. Flemming, R. Forbes, M. Fuentes, A. Geer, L. Haimberger, S. Healy, R. J. Hogan, E. Hólm, M. Janisková, S. Keeley, P. Laloyaux, P. Lopez, C. Lupu, G. Radnoti, P. Rosnay, I. Rozum, F. Vamborg, S. Villaume, J.-N. Thépaut, The ERA5 global reanalysis. *Q. J. Roy. Meteorol. Soc.* **146**, 1999–2049 (2020).
21. B. Martens, D. G. Miralles, H. Lievens, R. van der Schalie, R. A. M. de Jeu, D. Fernández-Prieto, H. E. Beck, W. A. Dorigo, N. E. C. Verhoest, GLEAM v3: Satellite-based land evaporation and root-zone soil moisture. *Geosci. Model Dev. Discuss.* **10**, 1903–1925 (2017).
22. D. Wu, X. Zhao, S. Liang, T. Zhou, K. Huang, B. Tang, W. Zhao, Time-lag effects of global vegetation responses to climate change. *Glob. Chang. Biol.* **21**, 3520–3531 (2015).
23. J. H. Kim, Multicollinearity and misleading statistical results. *Korean J. Anesthesiol.* **72**, 558–569 (2019).
24. S. Peng, S. Piao, P. Ciais, R. B. Myneni, A. Chen, F. Chevallier, A. J. Dolman, I. A. Janssens, J. Peñuelas, G. Zhang, S. Vicca, S. Wan, S. Wang, H. Zeng, Asymmetric effects of daytime and night-time warming on Northern Hemisphere vegetation. *Nature* **501**, 88–92 (2013).

25. D. R. Jensen, D. E. Ramirez, Revision: Variance inflation in regression. *Adv. Decis. Sci.* **2013**, 671204, 2013
26. A. E. Hoerl, R. W. Kennard, Ridge regression: Biased estimation for nonorthogonal problems. *Technometrics* **42**, 80–86 (2000).
27. A. Barkhordarian, K. W. Bowman, N. Cressie, J. Jewell, J. Liu, Emergent constraints on tropical atmospheric aridity—Carbon feedbacks and the future of carbon sequestration. *Environ. Res. Lett.* **16**, 114008 (2021).
28. S. H. Park, Collinearity and optimal restrictions on regression parameters for estimating responses. *Technometrics* **23**, 289–295 (1981).
29. J. Wang, F. Pan, J. Soininen, J. Heino, J. Shen, Nutrient enrichment modifies temperature-biodiversity relationships in large-scale field experiments. *Nat. Commun.* **7**, 13960 (2016).
30. A. N. Pettitt, A simple cumulative sum type statistic for the change-point problem with zero-one observations. *Biometrika* **67**, 79–84 (1980).
31. D. R. Woodruff, F. C. Meinzer, K. A. McCulloh, Height-related trends in stomatal sensitivity to leaf-to-air vapour pressure deficit in a tall conifer. *J. Exp. Bot.* **61**, 203–210 (2010).
32. D. K. Soni, S. Ranjan, R. Singh, P. B. Khare, U. V. Pathre, P. A. Shirke, Photosynthetic characteristics and the response of stomata to environmental determinants and ABA in *Selaginella bryopteris*, a resurrection spike moss species. *Plant Sci.* **207**, 191–192 (2012).
33. A. Sellin, M. Alber, M. Keinänen, P. Kupper, J. Lihavainen, K. Lõhmus, E. Oksanen, A. Sõber, J. Sõber, A. Tullus, Growth of northern deciduous trees under increasing atmospheric humidity: Possible mechanisms behind the growth retardation. *Reg. Environ. Change* **17**, 2135–2148 (2017).
34. A. Sellin, A. Tullus, A. Niglas, E. Õunapuu, A. Karusion, K. Lõhmus, Humidity-driven changes in growth rate, photosynthetic capacity, hydraulic properties and other functional traits in silver birch (*Betula pendula*). *Ecol. Res.* **28**, 523–535 (2013).
35. C. Grossiord, T. N. Buckley, L. A. Cernusak, K. A. Novick, B. Poulter, R. T. W. Siegwolf, J. S. Sperry, N. G. McDowell, Plant responses to rising vapor pressure deficit. *New Phytol.* **226**, 1550–1566 (2020).
36. J. L. Monteith, A reinterpretation of stomatal responses to humidity. *Plant Cell Environ.* **18**, 357–364 (1995).
37. V. Novák, J. Vidoň, Transpiration and nutrient uptake dynamics in maize (*Zea mays* L.). *Ecol. Model.* **166**, 99–107 (2003).
38. L. A. Cernusak, K. Winter, B. L. Turner, Transpiration modulates phosphorus acquisition in tropical tree seedlings. *Tree Physiol.* **31**, 878–885 (2011).
39. J. Lihavainen, V. Ahonen, S. Keski-Saari, A. Sõber, E. Oksanen, M. Keinänen, Low vapor pressure deficit reduces glandular trichome density and modifies the chemical composition of cuticular waxes in silver birch leaves. *Tree Physiol.* **37**, 1166–1181 (2017).
40. E. Oksanen, J. Lihavainen, M. Keinänen, S. Keski-Saari, S. Kontunen-Soppela, A. Sellin, A. Sõber. Northern Forest Trees Under Increasing Atmospheric Humidity. F. Cánovas, U. Lüttge, R. Matyssek, H. Pretzsch, Eds. Progress in Botany, vol 80. (Springer, Cham., 2018) https://doi.org/10.1007/124_2017_15
41. A. Niglas, P. Kupper, A. Tullus, A. Sellin, Responses of sap flow, leaf gas exchange and growth of hybrid aspen to elevated atmospheric humidity under field conditions. *AoB Plants* **6**, plu021 (2014).
42. F. Hayat, M. A. Ahmed, M. Zarebanadkouki, M. Javaux, G. Cai, A. Carminati, Transpiration Reduction in Maize (*Zea mays* L) in response to soil drying. *Front. Plant Sci.* **10**, 1695 (2020).
43. J. Martínez-Vilalta, R. Poyatos, D. Aguadé, J. Retana, M. Mencuccini, A new look at water transport regulation in plants. *New Phytol.* **204**, 105–115 (2014).
44. I. Jauregui, S. A. Rothwell, S. H. Taylor, M. A. J. Parry, E. Carmo-Silva, I. C. Dodd, Whole plant chamber to examine sensitivity of cereal gas exchange to changes in evaporative demand. *Plant Methods* **14**, 97 (2018).
45. J. Macková, M. Vašková, P. Macek, M. Hronková, L. Schreiber, J. Šantrůček, Plant response to drought stress simulated by ABA application: Changes in chemical composition of cuticular waxes. *Environ. Exp. Bot.* **86**, 70–75 (2013).
46. R. Schoppach, W. Sadok, Differential sensitivities of transpiration to evaporative demand and soil water deficit among wheat elite cultivars indicate different strategies for drought tolerance. *Environ. Exp. Bot.* **84**, 1–10 (2012).
47. S. Medina, R. Vicente, M. T. Nieto-Taladriz, N. Aparicio, F. Chairi, O. Vergara-Diaz, J. L. Araus, The plant-transpiration response to Vapor Pressure Deficit (VPD) in durum wheat is associated with differential yield performance and specific expression of genes involved in primary metabolism and water transport. *Front. Plant Sci.* **9**, 1994 (2019).
48. L. A. Cernusak, G. R. Goldsmith, M. Arend, R. T. W. Siegwolf, Effect of vapor pressure deficit on gas exchange in wild-type and abscisic acid–insensitive plants. *Plant Physiol.* **181**, 1573–1586 (2019).
49. J. Li, X. Li, Response of stomatal conductance of two tree species to vapor pressure deficit in three climate zones. *J. Arid. Land* **6**, 771–781 (2014).
50. G. Pasqualotto, V. Carraro, E. Suarez Huerta, T. Anfodillo, Assessment of canopy conductance responses to vapor pressure deficit in eight hazelnut orchards across continents. *Front. Plant Sci.* **12**, 767916 (2021).
51. T. N. Buckley, The control of stomata by water balance. *New Phytol.* **168**, 275–292 (2005).
52. P. J. Franks, Passive and active stomatal control: Either or both? *New Phytol.* **198**, 325–327 (2013).
53. P. J. Franks, G. D. Farquhar, The mechanical diversity of stomata and its significance in gas-exchange control. *Plant Physiol.* **143**, 78–87 (2007).
54. P. Cruiziat, H. Cochard, T. Améglio, Hydraulic architecture of trees: Main concepts and results. *Ann. For. Sci.* **59**, 723–752 (2002).
55. J. S. Sperry, Coordinating stomatal and xylem functioning – an evolutionary perspective. *New Phytol.* **162**, 568–570 (2004).
56. N. Martin-StPaul, S. Delzon, H. Cochard, Plant resistance to drought depends on timely stomatal closure. *Ecol. Lett.* **20**, 1437–1447 (2017).
57. N. G. McDowell, C. D. Allen, Darcy's law predicts widespread forest mortality under climate warming. *Nat. Clim. Change* **5**, 669–672 (2015).
58. X. Lian, S. Piao, A. Chen, K. Wang, X. Li, W. Buermann, C. Huntingford, J. Peñuelas, H. Xu, R. B. Myneni, Seasonal biological carryover dominates northern vegetation growth. *Nat. Commun.* **12**, 983 (2021).
59. J. K. Green, J. Berry, P. Ciais, Y. Zhang, P. Gentine, Amazon rainforest photosynthesis increases in response to atmospheric dryness. *Sci. Adv.* **6**, eabb7232 (2020).
60. Y. Zhang, J. Joiner, S. H. Alemohammad, S. Zhou, P. Gentine, A global spatially contiguous solar-induced fluorescence (CSIF) dataset using neural networks. *Biogeosciences* **15**, 5779–5800 (2018).
61. M. Jung, S. Koirala, U. Weber, K. Ichii, F. Gans, G. Camps-Valls, D. Papale, C. Schwalm, G. Tramontana, M. Reichstein, The FLUXCOM ensemble of global land-atmosphere energy fluxes. *Sci. Data* **6**, 74 (2019).
62. R. Gelaro, W. McCarty, M. J. Suárez, R. Todling, A. Molod, L. Takacs, C. A. Randles, A. Darmenov, M. G. Bosilovich, R. Reichle, K. Wargan, L. Coy, R. Cullather, C. Draper, S. Akella, V. Buchard, A. Conaty, A. M. da Silva, W. Gu, G. K. Kim, R. Koster, R. Lucchesi, D. Merkova, J. E. Nielsen, G. Partyka, S. Pawson, W. Putman, M. Rienecker, S. D. Schubert, M. Sienkiewicz, B. Zhao, The Modern-Era Retrospective Analysis for Research and Applications, Version 2 (MERRA-2). *J. Climate* **30**, 5419–5454 (2017).
63. T. Antonio, Z. Robert, *Global Aridity Index and Potential Evapotranspiration (ET0) Climate Database v2*. (2019).
64. X. Wang, P. Ciais, Y. Wang, D. Zhu, Divergent response of seasonally dry tropical vegetation to climatic variations in dry and wet seasons. *Glob. Chang. Biol.* **24**, 4709–4717 (2018).
65. G. Verstraeten, J. Poesen, G. Demarée, C. Salles, Long-term (105 years) variability in rain erosivity as derived from 10-min rainfall depth data for Ukkel (Brussels, Belgium): Implications for assessing soil erosion rates. *J. Geophys. Res. Atmos.* **111**, D22109 (2006).
66. X. Xu, D. Yang, H. Yang, H. Lei, Attribution analysis based on the Budyko hypothesis for detecting the dominant cause of runoff decline in Haihe basin. *J. Hydrol.* **510**, 530–540 (2014).

Acknowledgments

Funding: This work has been supported by the National Key Scientific Research and Development Program of China (grant 2017YFA0603601) and the Strategic Priority Research Program of the Chinese Academy of Sciences (grant XDA20060402). Support from the Swedish strategic research areas BECC and MERGE, as well as STINT (CH2020-8799 and CH2020-8767), are also acknowledged. **Author contributions:** B.H., Y.C., and Z.Z. designed the research. Z.Z., Y.D., R.T., X.X., and Y.Z. performed the analysis. Z.Z. and B.H. drafted the paper. Y.-P.W., H.W.C., D.C., Y.H.F., L.G., L.H., W.Y., X.H., H.L., and L.S. contributed to the interpretation of the results and to the writing of the paper. **Competing interests:** The authors declare that they have no competing interests. **Data and materials availability:** All data needed to evaluate the conclusions in the paper are present in the paper and/or the Supplementary Materials. The source data were freely accessed from the following locations: the CSIF dataset is from https://osf.io/8xqy6/. The LAI-MODIS dataset is from https://modis.gsfc.nasa.gov/data/. The FLUXCOM GPP dataset is from www.fluxcom.org/domains/fluxcom.org/CF-Products/. The ERA5 dataset is from https://cds.climate.copernicus.eu/cdsapp#!/dataset/reanalysis-era5-single-levels-monthly-means?tab=form. The GLEAM SM and transpiration data are from www.gleam.eu/#datasets. The MERRA-2 downward shortwave radiation dataset is from https://disc.gsfc.nasa.gov/datasets?project=MERRA-2. The AI dataset is from https://doi.org/10.6084/m9.figshare.7504448.v3. The source codes for conducting PLS-SEM can be obtained from the PLS-SEM Toolbox available on MATLAB Central File Exchange. The toolbox was downloaded on 6 February 2022 from the following URL: www.mathworks.com/matlabcentral/fileexchange/54147-pls-sem-toolbox.

Submitted 13 October 2022
Accepted 7 July 2023
Published 9 August 2023
10.1126/sciadv.adf3166